

RADRON: Cooperative Localization of Ionizing Radiation Sources by MAVs with Compton Cameras

Petr Stibinger¹ , Tomas Baca , Daniela Doubravova , Jan Rusnak ,
Jaroslav Solc , Jan Jakubek , Petr Stepan  and Martin Saska 

Abstract— We present a novel approach to localizing radioactive material by cooperating Micro Aerial Vehicles (MAVs). Our approach utilizes a state-of-the-art single-detector Compton camera as a highly sensitive, yet miniature detector of ionizing radiation. The detector’s exceptionally low weight (40 g) opens up new possibilities of radiation detection by a team of cooperating agile MAVs. We propose a new fundamental concept of fusing the Compton camera measurements to estimate the position of the radiation source in real time even from extremely sparse measurements. The data readout and processing are performed directly onboard and the results are used in a dynamic feedback to drive the motion of the vehicles. The MAVs are stabilized in a tightly cooperating swarm to maximize the information gained by the Compton cameras, rapidly locate the radiation source, and even track a moving radiation source.

I. INTRODUCTION

Nuclear environments represent a domain particularly well suited for the deployment of mobile robots [1]–[3]. The primary driving force is to reduce human exposure to harmful radiation, and to facilitate access to areas that are difficult to reach by conventional means. Unmanned Aerial Vehicles (UAVs) provide the capability to swiftly cover expansive areas, making them ideal for rapid response as well as repeated surveillance. Large aerial platforms offer higher payload capacity and operational endurance, while compact MAVs can operate much closer to the radiation sources, where the flux of ionizing particles is significantly denser. The reduced size and cost of smaller platforms open up a potential for multi-robot deployment, where the MAVs can operate in compact groups and act as a dynamic sensor network.

Nuclear environments can emerge suddenly—as a result of natural disasters, accidents, or criminal activities—or develop gradually through heavy industrial activity. In all cases, the terrain conditions are expected to be rugged and obstructed by debris, ongoing cleanup efforts, or nature reclaiming the depopulated areas. Aerial vehicles hold a clear advantage over ground-based platforms in rapid traversal of the area regardless of terrain conditions.

Continuous developments in radiation sensing technology have enabled the construction of extremely sensitive detectors, which are capable of distinguishing individual high-energy photons. This gave rise to a new type of sensors—Compton cameras—which utilize the predictable properties of Compton scattering [4] to determine a set of possible directions towards the radiation source. Compton cameras were pioneered in high-energy astronomy, and originally consisted of bulky scintillators and photomultipliers, which are impractical for use in aerial robotics. However, compact Compton

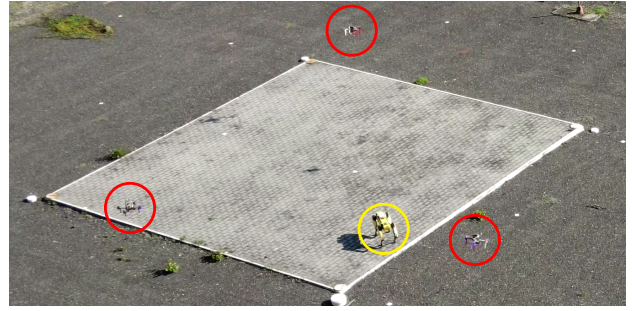


Fig. 1: Three cooperating MAVs localizing and tracking a moving radiation source. Each MAV (red) is equipped with a miniature Compton camera and an onboard computer. The ionizing radiation source (a sample of Cesium-137) is carried by a quadruped robot (yellow).

cameras are slowly becoming available [5], comprising of miniaturized scintillators [2], [6], [7] or semiconductor chips using direct energy conversion [8], [9].

A conventional Compton camera consists of two stacked detectors—a scatterer and an absorber. Such a configuration requires additional electronics for synchronization, and necessitates active cooling, making it impractical for use onboard an MAV. In this work, we exploit the cutting-edge advances in the semiconductor technology, which made a single-detector Compton camera possible. The reduced complexity makes this type of detector a great fit for sub-3 kg MAVs.

II. RELATED WORK

The area of the Fukushima Daiichi Nuclear Power Plant (FDNPP) has been inspected by several robotic missions since the disaster in 2011. Initial surveys were performed by UAVs equipped with powerful but heavy scintillator detectors [1], [2], [10], [11]. Similar missions were also conducted to monitor the environmental impact of uranium ore extraction at several mining sites [12]–[15]. In the aforementioned works, the authors rely on large UAVs which are only suitable for open areas where a Global Navigation Satellite System (GNSS) is available. However, recent advances in onboard sensing and GNSS-denied localization [16] have made it possible to deploy MAVs directly inside mine shafts [17], cave systems [18], and building interiors [19]–[21] including nuclear power plants [19].

The research on ionizing radiation localization is currently split into two major streams: the localization of discrete

radiation sources, and the identification of a continuous contamination by aerosols or dissolved nuclear material. The problem of discrete radiation source localization may be tackled by adapting well-known robotic principles such as maximum likelihood estimation [22], gradient descent [23], Kalman filters [24], and particle filters [25]–[27]. For spatially distributed radioactive fields, the aim is to estimate the spatial representation of the radiation field and its volumetric properties. Related research has demonstrated feasible approaches using a Gaussian mixture model [28], maximum likelihood estimation [29], contour analysis [10], [30], and gradient descent [31], [32].

The localization approaches often rely on teleoperation [33], or following pre-planned waypoints [1], [34]–[37]. An active approach, utilizing a grid-based Bayesian estimator in a direct motion planning feedback loop, is presented in [10] using a 90 kg UAV. The approach in [11] employs a cooperative approach, using a 94 kg UAV following a space-filling path to map the area of interest and to identify radiation hotspots for further inspection by a companion Unmanned Ground Vehicle (UGV). Similar work was presented in [38], where a 16.8 kg UAV is used for exhaustive aerial mapping, and an autonomous companion UGV is later deployed for a close-up hotspot inspection. In [39] a large eight-rotor UAV capable of carrying up to 16 kg of payload is used. The authors use a heavy gamma spectrometer, enabling the localization of multiple radiation sources in a semi-autonomous mode. In [3], a small 2.6 kg six-rotor MAV equipped with a scintillation detector employs an active radiation search strategy, using information gain and distance from the radiation field centroid in further path-planning. The authors of [40] demonstrate an informative path planning and characterization of a distributed radiation field by a single MAV weighing just 639 g. Contrary to our approach, both the platform and methodology in [40] are heavily optimized for indoor deployment and an operational time < 6 min. In [41], a method for localizing multiple sources of radiation by a team of MAVs is introduced. Nonetheless, their approach treats the MAVs as independent agents operating in a shared map, thus not fully exploiting the information from concurrent measurements taken at different locations.

The simulations in [24], [42] demonstrate, that a single MAV may be used to follow a moving radiation source under certain conditions. However, there is a consensus that multiple networked sensors are required to accurately track a moving radiation source [43]–[45]. To the best of our knowledge, cooperative localization and tracking of a moving ionizing radiation source has not been tackled in the existing literature. This work distinguishes itself from the state of the art by leveraging a team of networked, tightly cooperating MAVs to localize and track the radiation source.

III. CONTRIBUTION

We contribute a decentralized multi-robot approach for localizing an ionizing radiation source that diverges from the conventional approaches relying on a single, heavy platform. Our solution uniquely combines the compact, extremely

lightweight MiniPIX TPX3 Compton camera with a self-organized swarm of tightly cooperating MAVs, enabling deployment in environments previously inaccessible to systems relying on bulky detectors and robots. We extend the Compton data fusion method from [24] to the multi-robot domain and introduce a novel control law that uses distributed radiation measurements processed in real time to dynamically drive the motion of the swarm. The problem represents a rare instance where the use of a tightly cooperating self-organized swarm is fundamentally justified, as our unique approach fully utilizes the availability of distributed radiation measurements processed directly onboard. This removes the need to perform long exposition imaging, which would be otherwise necessary with miniaturized radiation sensors, and results in a key advantage—the ability to localize and track a moving radiation source in real time. This capability is not attainable, or is severely limited with the state-of-the-art single-vehicle methods. We empirically validate all stated capabilities in realistic simulations, as well as real-world experiments.

IV. MEASUREMENT AND DATA FUSION

A. Single-detector Compton camera

The MiniPIX TPX3 Compton camera leverages the predictable mechanics of Compton scattering to estimate the direction of incoming ionizing radiation. Compton scattering occurs when a high-energy photon interacts with a charged particle, typically an electron. During this interaction, the photon transfers a portion of its energy to the charged particle, and scatters in a new direction. The energy of the scattered photon $E_{\lambda'}$ is derived from [4] as:

$$E_{\lambda'} = \frac{E_{\lambda}}{1 + (E_{\lambda}/(m_e c^2))(1 - \cos \theta)}, \quad (1)$$

where E_{λ} is the initial photon energy, m_e is the rest mass of an electron, c is the speed of light in vacuum, and θ is the scattering angle. The initial energy E_{λ} is unknown, however, the conservation of energy for the scattering event holds:

$$E_{\lambda} = E_{\lambda'} + E_{e'}, \quad (2)$$

where $E_{e'}$ is the energy of the recoiled electron. If the recoiled electron and scattered photon are detected, it is possible to reconstruct the scattering angle θ as:

$$\theta = \arccos \left(1 + m_e c^2 \left(\frac{1}{E_{\lambda}} - \frac{1}{E_{\lambda'}} \right) \right). \quad (3)$$

The Timepix3 chip inside the camera consists of a 256×256 pixel grid on a $14 \text{ mm} \times 14 \text{ mm}$ CdTe chip. Each pixel operates as an independent radiation detector capable of direct energy conversion. The 2D position of both scattering products can be accurately determined from the indices of activated pixels. Additionally, it is possible to infer the relative distance between the scattering products from the difference in detection times and the velocity of signal propagation through the detector. The velocity is obtained from a calibration process with nanosecond precision [24], [46].

As the third coordinate cannot be measured in absolute terms, an assumption is made, that the Compton scattering

occurs directly on the outer edge of the detector. This yields the 3D coordinates $\mathbf{c}_{e'}$, $\mathbf{c}_{\lambda'}$ for the recoiled electron and the scattered photon, respectively. Finally, the Compton cone \mathbb{C} is reconstructed (Fig. 2). The cone axis is given by $\mathbf{c}_{e'}$, $\mathbf{c}_{\lambda'}$, the apex angle θ is given by (3), and the apex point coincides with $\mathbf{c}_{e'}$. The surface of the cone represents a set of possible origins of the incoming ionizing radiation. The assumption made here does not influence the shape of the cone, it only shifts it along the detector's z -axis. The detector thickness in this direction is only 2 mm, therefore the error introduced is negligible when considering the real-world distances involved in target localization by MAVs.

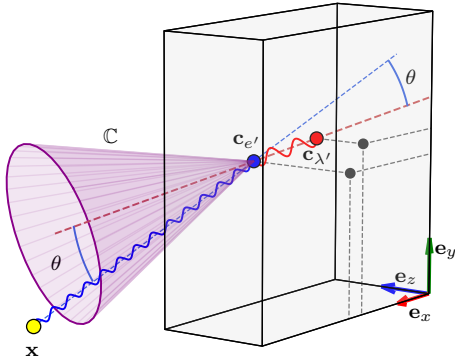


Fig. 2: Cone reconstruction in a single-detector Compton camera. A high-energy photon (blue) is emitted by a source \mathbf{x} . The Compton scattering occurs on the first contact with the detector and the recoiled electron is immediately absorbed. The scattered photon (red) passes through the detector until it is also absorbed. Energies $E_{\lambda'}$, $E_{e'}$ are measured directly by the pixel matrix bonded to the rear face of the detector. The active pixels pinpoint the x , y coordinates of both events $\mathbf{c}_{e'}$, $\mathbf{c}_{\lambda'}$. The difference in z is computed from the time delay between the two detection events and the velocity of event propagation (obtained in calibration). The scattering angle θ is computed using (3). Finally, a set of all possible origins of the high-energy photon is reconstructed. This set forms the surface of a cone \mathbb{C} .

B. Data fusion for multiple Compton cameras

The position of a radiation source is conventionally estimated by projecting the Compton cones into a simple geometric approximation of the environment, such as a 2D projection plane [7], [46], a sphere centered around the detector [47], or a 3D voxel grid [29]. However, such approaches require long-exposure imaging with a stationary Compton camera. This strategy is not feasible for compact MAVs with a limited operational time. Instead, we exploit the mobility of the MAVs and employ a novel approach to Compton cone fusion, which enables rapid estimation from only a few samples. The approach relies on event-based processing of individual Compton scattering occurrences while the MAV is moving through the environment at high speed.

Our data fusion method relies on the Linear Kalman Filter (LKF), which is well suited for single-target localization.

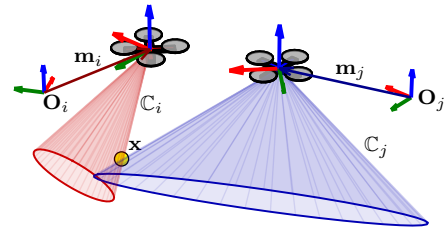


Fig. 3: An example with 2 MAVs using heterogeneous positioning systems. Each drone i , j estimates its position and orientation relative to the origin \mathbf{O}_i , \mathbf{O}_j , respectively. The Compton cones \mathbb{C}_i , \mathbb{C}_j are also projected in the respective coordinate frames. Under (A2), the position of the radiation source \mathbf{x} can be estimated in both coordinate frames using all available measurements.

Additionally, the algorithm is computationally inexpensive, which is crucial for real-time onboard estimation performed by a resource-constrained MAV. Due to the limited information provided by isolated measurements, we do not model the dynamics of the target in the estimation process, and instead utilize the track-by-detection approach. Therefore, the state-space model of the radiation source is reduced to:

$$\mathbf{x}_k = \mathbf{F}\mathbf{x}_{k-1}, \quad (4)$$

where $\mathbf{x}_k = [x_x \ x_y \ x_z]^T$ is the estimated position of the radiation source at step k , and \mathbf{F} is an identity matrix $\mathbf{I}_{3 \times 3}$. To input a new measurement to the LKF, the Compton cone \mathbb{C} has to be transformed into a vector, as closer described in [24]. Here, we generalize the process so that an arbitrary number of detectors and robots can be used simultaneously. In the following text, we refer to the position of the radiation source estimated by the LKF as a *hypothesis*. The generalization is done under the following assumptions:

- (A1) MAV i estimates its own position and orientation in the environment as \mathbf{m}_i relative to the origin \mathbf{O}_i .
- (A2) A transformation $\mathbf{T}_{i,j}$ exists between the coordinate frames used by MAVs i , j , s.t. $\mathbf{m}_j = \mathbf{T}_{i,j}\mathbf{m}_i$.
- (A3) The optimal measurement correction places the current hypothesis \mathbf{x}_k to the nearest point on the surface of the cone \mathbb{C}_k .

The assumptions (A1), (A2) permit the use of heterogeneous positioning systems within the swarm, as illustrated in Fig. 3. Under these assumptions, all MAVs are able to utilize the full set of measurements collected by the swarm, and perform the data fusion and motion planning directly onboard.

The geometric representation of (A3) depends on the orientation of \mathbb{C} , and is either the apex of the cone, or an orthogonal projection of the previous hypothesis \mathbf{x}_{k-1} onto the surface of the cone (6). To compute the orthogonal projection (Fig. 4), let \mathbf{u} , \mathbf{v} be unit vectors originating at the cone's apex $\mathbf{c}_{e'}$. Vector \mathbf{u} is collinear with the axis of the cone and \mathbf{v} is oriented towards \mathbf{x}_{k-1} . These two vectors unambiguously define a plane in 3D. The angle α between

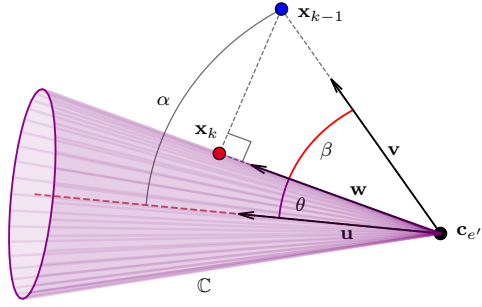


Fig. 4: Measurement correction done by projecting the latest hypothesis x_{k-1} onto the surface of a cone \mathbb{C} to get a corrected hypothesis x_k .

u and v is then given as:

$$\alpha = \arccos(u \cdot v) = \theta + \beta, \quad (5)$$

where θ is the scattering angle and β is the angle between the surface of cone \mathbb{C} and v . Rotating v by the angle $-\beta$ yields vector w . The hypothesis x_k is projected orthogonally on the surface of \mathbb{C} . Finally, x_k forms a right-angled triangle with x_{k-1} and $c_{e'}$, and x_k is then computed as:

$$x_k = \begin{cases} c_{e'} + w \cdot \|x_{k-1} - c_{e'}\| \cdot \cos \beta, & \text{if } \alpha < \pi/2, \\ c_{e'}, & \text{otherwise.} \end{cases} \quad (6)$$

Since the orthogonal projection moves the hypothesis in a known direction, we model the measurement covariance \mathbf{R} accordingly in each correction step of the LKF. A canonical covariance matrix $\mathbf{R}_{\mathbb{C}}$ is created with the measurement covariance ρ assigned to the first coordinate. The other elements on the main diagonal are assigned values orders of magnitude larger than ρ . A rotation \mathbf{P} is then applied, s.t. the X-axis is collinear with the projection axis ($x_k - x_{k-1}$). The result is a covariance matrix \mathbf{R} that only increases the estimate confidence along the axis of orthogonal projection:

$$\mathbf{R}_{\mathbb{C}} = \begin{pmatrix} \rho & 0 & 0 \\ 0 & \rho \cdot 10^4 & 0 \\ 0 & 0 & \rho \cdot 10^4 \end{pmatrix}, \quad \mathbf{R} = \mathbf{P} \mathbf{R}_{\mathbb{C}} \mathbf{P}^T. \quad (7)$$

V. COOPERATIVE LOCALIZATION STRATEGY

This section outlines the novel cooperative radiation source localization strategy using a swarm of MAVs. The mission is divided into two distinct stages: an initial systematic search aimed at quickly acquiring an approximate position of the source, and a cooperative tracking phase where the MAV swarm dynamically centers itself on the hypothesis and continuously refines the estimate. A key aspect is the decentralized control and estimation pipeline, where each MAV performs its own data fusion and motion planning onboard, enabled by sharing the Compton measurements and MAV positions among all swarm members.

A. Hypothesis initialization

The initial stage focuses on rapidly acquiring the initial hypothesis x_0 to initialize the LKF. The data fusion approach described in Sec. IV relies on recursive projection of the

previous hypothesis onto the surface of a new Compton cone. Since individual Compton measurements do not convey any information about the distance between the detector and the radiation source, the initialization has to be performed by gathering M measurements taken at different locations.

The area of interest is divided into N equal segments, and a space-filling path is generated for each segment. Each MAV is then assigned one path to explore one segment of the area. While the systematic search is ongoing, the MAVs maintain a fixed velocity and continuously change their heading to minimize potential blind spots of the forward-mounted Compton cameras. During this stage, the MAVs operate independently, but share all Compton measurements with the other vehicles.

Once the cumulative amount of Compton cones reaches M , the initial hypothesis x_0 is computed. This computation is formulated as a non-linear least squares optimization task to find a point that minimizes the squared distance to all the surfaces of the M cones. The formulation of the optimization task is detailed in [24]. Solving the optimization task is computationally intensive, therefore, it is only performed once to acquire x_0 .

B. Cooperative source localization and tracking

Upon acquiring x_0 , the mission enters the second stage where all MAVs operate as a tightly cooperating, self-organized swarm. At this stage, the goal is to maximize the information gained by the miniature Compton cameras and to continuously update the hypothesis, enabling the swarm to localize and track the radiation source.

A single Compton camera event yields a set of possible directions towards the radiation source. This set can be narrowed down by consecutive measurements. However, even a long-exposure imaging by a stationary camera capturing thousands of events, will only yield a direction vector towards the radiation source. Moreover, the estimation may converge at a local optimum located at the position of the Compton camera itself, as all cones have their apex points concentrated on the miniature surface of the detector. Therefore, it is necessary to keep the cameras in motion, so that subsequent measurements are taken at different points in the environment.

Following a circular path centered at the hypothesis ensures, that the camera moves orthogonally to the direction to the hypothesis, and the baseline between consecutive measurements is maximized. Using more than one MAV increases the overall sensor volume and inherently provides measurements from multiple viewpoints. This dramatically enhances the sensitivity and the ability to track a moving radiation source. The simultaneous use of multiple MAVs necessitates a high-level controller to coordinate motion and efficiently distribute the Compton cameras. We implement a novel decentralized flocking control leveraging the computationally inexpensive data fusion approach introduced in Sec. IV. Each swarm member performs the fusion directly onboard, using the results in feedback for motion planning.

TABLE I: Notation used in the flocking algorithm description

N	number of MAVs in the swarm
r	desired circle radius
v	desired tangential speed
K	number of trajectory generation steps
$\mathbf{t}_i[k]$	k -th trajectory step of the i -th MAV
\mathbf{x}	estimated position of the radiation source (hypothesis)
$\mathbf{m}_i = (r_i \ \varphi_i)^T$	position of the i -th MAV in polar coordinates
θ_i	smallest angle from the i -th MAV to another MAV
θ^*	uniform spacing angle

C. Compton-driven flocking

The flocking controller aims to distribute the MAVs on a circle around the hypothesis while maintaining a desired radius r and tangential speed v . The core objective is to achieve a uniform spacing angle $\theta^* = (2\pi/N)$ rad between neighboring MAVs to maximize the baseline between the Compton cameras.

The Compton cones reconstructed from individual measurements, along with the current position estimates, are shared between the MAVs. Under assumption (A2), each MAV can utilize this data within its own frame of reference. This ensures all MAVs operate with the same hypothesis and plan their own path on the same circle.

The radioactive object is assumed to be a point source located on the surface of the environment, with a uniform spatial distribution of radiation. The flocking algorithm therefore focuses on the horizontal motion of the MAVs, assuming they all operate at the same height above ground. We describe the problem in the plane of encirclement using polar coordinates with the hypothesis \mathbf{x} placed at the origin. We utilize a trajectory generation approach rather than a traditional feedback controller, due to the step-like disturbances introduced by the irregular updates of the hypothesis by the LKF, which occur with each new Compton cone reconstruction. Each swarm member is assigned a unique ID $i \in \{1, \dots, N\}$, and the positions of the MAVs are $\mathbf{m}_i = [r_i, \varphi_i]^T$.

The trajectory is generated for a single-vehicle as a circular arc with radius r . The arc is divided into K samples using an arbitrary sampling period ΔT to achieve a desired tangential speed v . To enforce uniform distribution of the MAVs on a circle, the trajectories are offset using a bias angle β_i . Firstly, the angle θ_i is computed as the smallest oriented angle between the i -th MAV and its neighbors:

$$\theta_i = \text{AngleDiff}(\mathbf{m}_i, \mathbf{m}_j), \quad (8)$$

where j is the index of the i -th MAV's nearest neighbor in terms of the central angle φ :

$$j = \underset{j \in N \setminus i}{\text{argmin}} |\text{AngleDiff}(\mathbf{m}_i, \mathbf{m}_j)|. \quad (9)$$

The bias β_i is then applied in the direction opposite to θ_i , acting as a repulsive force between the swarm members:

$$\beta_i = -\text{sgn}(\theta_i) \beta. \quad (10)$$

Finally, the desired trajectory \mathbf{t}_i is generated as a sequence:

$$\mathbf{t}_i[k] = [r, \varphi_i + \beta_i + krv\Delta T]^T, \forall k \in \{0, \dots, K\}. \quad (11)$$

Without loss of generality, the process of trajectory generation can be illustrated for a 2-vehicle case (Fig. 5). It is worth noting, that the initial point of the trajectory $\mathbf{t}_i[0]$ may not coincide with the current position of the MAV \mathbf{m}_i . The discontinuity is tackled by passing the desired trajectory through the MPC trajectory tracker [48] further in the control pipeline. The tracker then outputs a feasible tracking reference for the MAV's flight controller. The resulting control reference satisfies the vehicle's velocity and acceleration constraints and is optimal with respect to the tracker's dynamic model. The complete flow of data within one MAV is shown in Fig. 6.

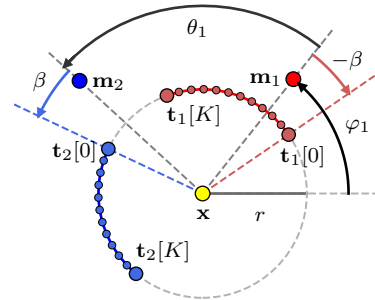


Fig. 5: A top-down view of the swarm's self-organization during the encirclement of the hypothesis. Here shown for two MAVs with starting positions $\mathbf{m}_1, \mathbf{m}_2$. The signed angle from \mathbf{m}_1 to the nearest other MAV is θ_1 . To steer the swarm towards a uniform spacing angle θ^* , a bias β is applied to the start of the generated trajectory \mathbf{t}_1 . The bias is applied in the orientation opposite to θ . The first point of the desired trajectory $\mathbf{t}_1[0]$ does not correspond to the position of the MAV \mathbf{m}_1 . However, the discontinuities in the desired trajectory are already tackled at a lower level of the control architecture [48]. This allows the swarm controller to retain simplicity and generate new trajectories at a high rate.

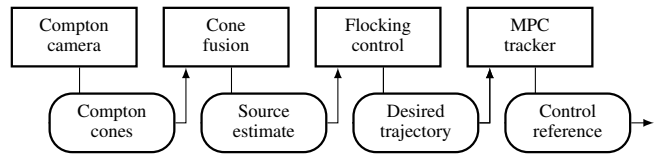


Fig. 6: A data flow diagram for one of the MAVs. The decentralized flocking control is driven by the fusion of radiation measurements from all swarm members performed onboard each vehicle in real time. This allows the system to rapidly react to sudden changes, such as the movement of the radiation source. The desired trajectory is passed through the MPC trajectory tracker [48] which ensures the control reference is feasible with respect to the dynamic constraints of the vehicle.

VI. SIMULATIONS

This section presents a series simulations designed to rigorously evaluate the novel cooperative radiation localization strategy introduced in Sec. V. The primary goal is to validate the capabilities of the proposed system and to highlight the

advantages of using a swarm over a single MAV. Additionally, we focus on tuning the control parameters, notably the encirclement radius r , tangential speed v , and swarm size N , to outline a suitable configuration for real-world deployment.

A. Swarm stabilization

A series of simulations was designed to validate that the proposed flocking controller (11) is capable of stabilizing the swarm from an unorganized initial state and recover after a step disturbance. We decouple the Compton cone fusion from the motion planning, and use a static hypothesis in this simulation series. The MAVs are initially placed at an arbitrary position and the flocking controller is engaged. A disturbance is introduced by changing the position of the hypothesis by 10 m with a 60 s period. The disturbance shifts the center of the circular trajectory and forces the swarm to reorganize. The results (Fig. 7) indicate that the flocking controller is able to stabilize the swarm in the circular motion, achieve the desired speed v , and uniformly distribute the MAVs around the hypothesis.

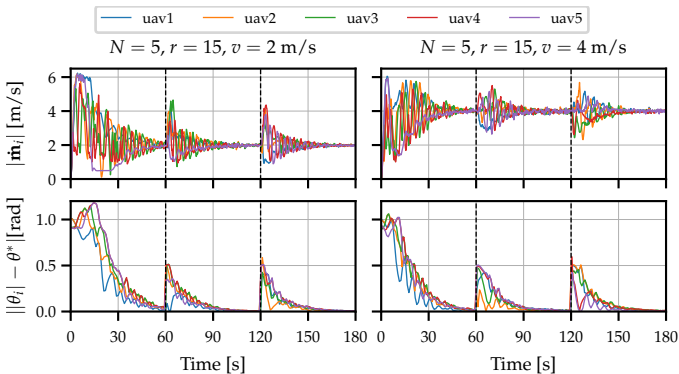


Fig. 7: Simulation results showing the swarm stabilizing after a step disturbance. The flocking algorithm is initialized with 5 MAVs in arbitrary positions. The hypothesis is static and every 60 seconds its position is shifted, forcing the swarm to reorganize around a new center. The upper row shows the instantaneous speed $|\dot{m}_i|$ of the MAVs. The lower row shows the magnitude of difference between the uniform spacing angle θ^* and the relative angle θ_i to the nearest neighbor of each MAVs. The speed of all MAVs converges at the desired speed v , and the angular spacing converges to a uniform distribution.

B. Radiation source localization

Building on the capabilities of a self-stabilizing MAV swarm, this section tackles the core objective: the cooperative radiation source localization. Through a series of realistic simulations, we validate the system's effectiveness in localization and tracking of a moving radiation source, and highlight the key advantages over the state-of-the-art single-vehicle methods. The simulations are performed in a 100×100 m area. A cooperative approach using a 3 MAVs is compared to the single-MAV approach using the same control parameters: $r = 12$ m, $v = 3$ m s $^{-1}$, $K = 30$. The radiation source is Cesium-137 with activity 3 GBq,

and for the tracking experiments it follows a circular path with a 40 m radius at a speed of 1 m s $^{-1}$. We focus on the comparative qualities of both mission stages: hypothesis initialization and radiation source tracking. The simulation is terminated when a Compton cone is not received for more than 20 s, indicating a loss of the target, or after 180 s of continuous tracking. The simulation is repeated 50 times for each configuration, with randomized initial position of the radiation source, to enable both quantitative and qualitative evaluation. The simulation results are summarized in Tab. II and clearly highlight the comparative advantages of the MAVs swarm over a single MAV in localizing both static and moving radiation sources. With the novel swarm approach, the time to acquire the initial hypothesis is dramatically reduced to just 25% of the single-vehicle requirement. It is also worth noting, that the median estimation error of a single vehicle reaches over 20 m when the radiation source is moving, which significantly limits any practical use of this approach. The use of a swarm, on the other hand, improves the accuracy of tracking a moving source by nearly 300%, and the median error achieved by a swarm of just 3 MAVs would be sufficient to pinpoint a specific vehicle.

TABLE II: Localization and tracking simulation results

	Static source		Moving source	
	Solo	Swarm	Solo	Swarm
Time to \mathbf{x}_0 (median)	329.63 s	59.16 s	203.66 s	52.90 s
Time to \mathbf{x}_0 (max)	584.67 s	124.68 s	359.30 s	149.70 s
Tracking time (average)	167.01 s	180 s	44.50 s	133.30 s
Tracking time (max)	180 s	180 s	122.43 s	180 s
Estimation error (median)	2.59 m	2.26 m	20.34 m	6.70 m

VII. EXPERIMENTS

A series of experiments was conducted to evaluate the localization capabilities in real-world conditions utilizing 3 MAVs built on the modular hardware platform [49]. The core software stack is the MRS UAV System [16] with ROS¹ Noetic running on the Intel NUCi7 onboard computer. The sensor payload consists of a MiniPIX TPX3 miniature Compton camera with a 2 mm CdTe detector, a Holybro Pixhawk4 flight controller, a Garmin LIDAR-Lite v3 rangefinder used as altimeter, and a NEO-M8N GNSS receiver (Fig. 8a).

The radioactive sources used in the experiments are laboratory isotopes of Cesium-137 with activity² 179 MBq and 2 GBq. The position of the radiation source is chosen randomly for each experiment and the ground truth is measured using GNSS or estimated from a bird's-eye view footage of the experiment. The search is conducted in an open area 40 m \times 50 m in size with no obstacles, and only one radiation source is present at a time.

For the experiments with a moving radiation source, the 2 GBq Cesium-137 sample was carried by a remotely controlled Boston Dynamics Spot (Fig. 8b). The motion of the radiation source consisted of ad-hoc straight and curved

¹<https://www.ros.org/>

²1 Bq = 1 nuclear decay event per second

segments taken at various speeds, and focused on finding the tracking limits in real-world conditions. The moving source experiment was performed 7 times resulting in over 60 min of accumulated flight data from each device. The results of the experiments are summarized in Tab. III. Our approach was found to be capable of tracking the motion of the 2 GBq source up to a speed of 3 m s^{-1} using 3 MAVs. If using just 1 or 2 MAVs, the system was not able to localize and follow the source moving at this speed in any of the attempts we tried. Fig. 9 shows snapshots of the moving source experiments, highlighting the flight paths, estimated position of the radiation source, and the ground truth.

TABLE III: Performance evaluation of the real-world deployment using 3 MAVs and Cesium-137 as the radiation source.

	179 MBq	2 GBq	2 GBq (moving)
Time to x_0 (median)	105.46 s	29.55 s	45.88 s
Time to x_0 (max)	115.88 s	34.80 s	139.98 s
Estimation error (median)	2.65 m	3.49 m	3.50 m
Estimation error (average)	5.04 m	4.89 m	6.24 m

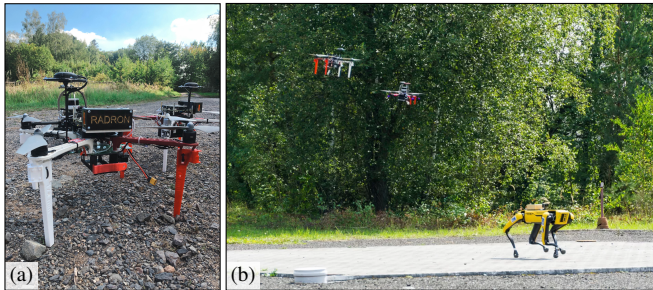


Fig. 8: Photos taken during the real-world experiments showing the MAV platforms (a) with the MiniPIX TPX3 Compton camera mounted on the front. To shield the sensitive electronics from dust, the Compton camera is sealed in a 3D-printed case (black) which gamma rays easily penetrate. For the mobile source tracking experiments (b), the radiation source was carried by the Boston Dynamics Spot legged robot.

VIII. CONCLUSION

The simulation and experimental results conclusively demonstrate a clear advantage of a cooperating MAV swarm over a single vehicle across all performance metrics for radiation source localization. The superiority is clearly rooted in the fusion of measurements taken from multiple viewpoints simultaneously, which results in significant speed up of the initialization phase and dramatic improvements in source localization accuracy. A truly unique aspect of our novel approach is the ability to localize and track a moving radiation source. The empirical results highlight the critical importance of the initialization phase, as a poor initial hypothesis may prevent the subsequent estimation and tracking method from converging due to an insufficient rate of radiation events reaching the Compton cameras.

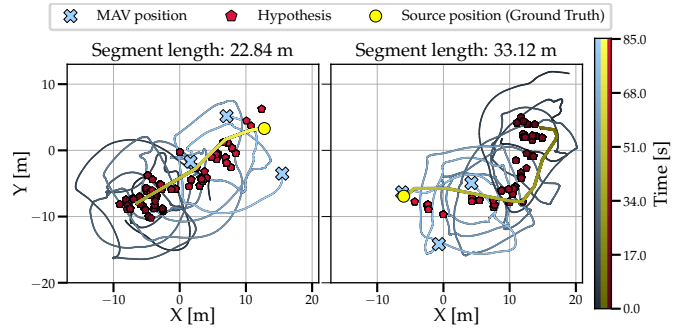


Fig. 9: A top-down view of the moving radiation source experiments. The radiation source is carried by a remotely controlled ground robot. The estimated position of the source (hypothesis) is shown in red, and the path taken by the MAVs is shown in blue. The change in color brightness illustrates the time progression of the experiments.

REFERENCES

- [1] Y. Sanada and T. Torii, “Aerial radiation monitoring around the fukushima dai-ichi nuclear power plant using an unmanned helicopter,” *Journal of environmental radioactivity*, vol. 139, pp. 294–299, 2015.
- [2] J. Jiang *et al.*, “A prototype of aerial radiation monitoring system using an unmanned helicopter mounting a gagg scintillator compton camera,” *Journal of Nuclear Science and Technology*, vol. 53, no. 7, pp. 1067–1075, 2016.
- [3] F. Mascarich, T. Wilson, C. Papachristos, and K. Alexis, “Radiation source localization in gps-denied environments using aerial robots,” in *IEEE ICRA*, 2018.
- [4] A. H. Compton, “A quantum theory of the scattering of x-rays by light elements,” *Physical review*, vol. 21, no. 5, p. 483, 1923.
- [5] R. K. Parajuli, M. Sakai, R. Parajuli, and M. Tashiro, “Development and applications of compton camera—a review,” *Sensors*, vol. 22, no. 19, p. 7374, 2022.
- [6] Y. Sato, Y. Tanifuji, Y. Terasaka, H. Usami, M. Kaburagi, K. Kawabata, W. Utsugi, H. Kikuchi, S. Takahira, and T. Torii, “Radiation imaging using a compact compton camera inside the fukushima daiichi nuclear power station building,” *Journal of Nuclear Science and Technology*, vol. 55, no. 9, pp. 965–970, 2018.
- [7] Y. Sato, Y. Terasaka, W. Utsugi, *et al.*, “Radiation imaging using a compact Compton camera mounted on a crawler robot inside reactor buildings of Fukushima Daiichi Nuclear Power Station,” *Journal of Nuclear Science and Technology*, vol. 56, no. 9-10, pp. 801–808, 2019.
- [8] S. Watanabe, S. Takeda, S.-n. Ishikawa, H. Odaka, M. Ushio, T. Tanaka, K. Nakazawa, T. Takahashi, H. Tajima, Y. Fukazawa, *et al.*, “Development of semiconductor imaging detectors for a si/cdte compton camera,” *Nuclear Instruments and Methods in Physics Research Section A: Accelerators, Spectrometers, Detectors and Associated Equipment*, vol. 579, no. 2, pp. 871–877, 2007.
- [9] D. Turecek, J. Jakubek, E. Trojanova, and L. Sefc, “Compton camera based on timepix3 technology,” *Journal of Instrumentation*, vol. 13, no. 11, p. C11022, 2018.
- [10] J. Towler, B. Krawiec, and K. Kochersberger, “Radiation mapping in post-disaster environments using an autonomous helicopter,” *Remote Sensing*, vol. 4, no. 7, pp. 1995–2015, 2012.
- [11] G. Christie, A. Shoemaker, K. Kochersberger, P. Tokek, L. McLean, and A. Leonessa, “Radiation search operations using scene understanding with autonomous uav and ugv,” *Journal of Field Robotics*, vol. 34, no. 8, pp. 1450–1468, 2017.
- [12] P. Martin, O. Payton, J. Fardoulis, *et al.*, “The use of unmanned aerial systems for the mapping of legacy uranium mines,” *Journal of environmental radioactivity*, vol. 143, pp. 135–140, 2015.
- [13] O. Salek, M. Matolin, and L. Gryc, “Mapping of radiation anomalies using UAV mini-airborne gamma-ray spectrometry,” *Journal of environmental radioactivity*, vol. 182, pp. 101–107, 2018.
- [14] A. Keatley, P. Martin, K. Hallam, O. Payton, R. Awbery, F. Carvalho, J. Oliveira, L. Silva, M. Malta, and T. Scott, “Source identification of uranium-containing materials at mine legacy sites in Portugal,” *Journal of Environmental Radioactivity*, vol. 183, pp. 102–111, 2018.

[15] C. Kunze, B. Preugschat, R. Arndt, F. Kandzia, B. Wiens, and S. Altfelder, "Development of a uav-based gamma spectrometry system for natural radionuclides and field tests at central asian uranium legacy sites," *Remote Sensing*, vol. 14, no. 9, p. 2147, 2022.

[16] T. Baca, M. Petrlik, M. Vrba, V. Spurny, R. Penicka, D. Hert, and M. Saska, "The mrs uav system: Pushing the frontiers of reproducible research, real-world deployment, and education with autonomous unmanned aerial vehicles," *Journal of Intelligent & Robotic Systems*, vol. 102, no. 1, pp. 1–28, 2021.

[17] T. Rouček, M. Pecka, P. Čížek, T. Petříček, J. Bayer, V. Šalanský, D. Heřt, M. Petrlik, T. Báča, V. Spurný, *et al.*, "Darpa subterranean challenge: Multi-robotic exploration of underground environments," in *International Conference on Modelling and Simulation for Autonomous Systems*. Springer, 2019, pp. 274–290.

[18] M. Petrlik, T. Baca, D. Hert, M. Vrba, T. Krajník, and M. Saska, "A Robust UAV System for Operations in a Constrained Environment," *IEEE Robotics and Automation Letters*, vol. 5, 4 2020.

[19] V. Kratky, P. Petracek, *et al.*, "Autonomous reflectance transformation imaging by a team of unmanned aerial vehicles," *IEEE Robotics and Automation Letters*, vol. 5, no. 2, pp. 2302–2309, 4 2020.

[20] M. Saska, D. Hert, T. Baca, V. Kratky, and T. Nascimento, "Formation Control of Unmanned Micro Aerial Vehicles for Strained Environments," *Autonomous Robots*, pp. 1573–7527, 2020.

[21] V. Pitzl, P. Stepan, and M. Saska, "Autonomous flying into buildings in a firefighting scenario," in *2021 IEEE International Conference on Robotics and Automation (ICRA)*. IEEE, May 2021, pp. 239–245.

[22] G. Cordone, R. R. Brooks, S. Sen, N. S. Rao, C. Q. Wu, M. L. Berry, and K. M. Grieme, "Improved multi-resolution method for mle-based localization of radiation sources," in *2017 20th International Conference on Information Fusion (Fusion)*. IEEE, 2017, pp. 1–8.

[23] H. E. Baidoo-Williams, S. Dasgupta, R. Mudumbai, and E. Bai, "On the gradient descent localization of radioactive sources," *IEEE Signal Processing Letters*, vol. 20, no. 11, pp. 1046–1049, 2013.

[24] T. Baca, P. Stibinger, D. Doubravova, D. Turecek, J. Solc, J. Rusnak, M. Saska, and J. Jakubek, "Gamma Radiation Source Localization for Micro Aerial Vehicles with a Miniature Single-Detector Compton Event Camera," in *2021 International Conference on Unmanned Aircraft Systems (ICUAS)*. IEEE, June 2021, pp. 338–346.

[25] W. Gao, W. Wang, H. Zhu, G. Huang, D. Wu, and Z. Du, "Robust radiation sources localization based on the peak suppressed particle filter for mixed multi-modal environments," *Sensors*, vol. 18, no. 11, p. 3784, 2018.

[26] N. Pinkam, A. Elibol, and N. Y. Chong, "Informative mobile robot exploration for radiation source localization with a particle filter," in *2020 Fourth IEEE International Conference on Robotic Computing (IRC)*. IEEE, 2020, pp. 107–112.

[27] R. B. Anderson, M. Pryor, A. Abeyta, and S. Landsberger, "Mobile robotic radiation surveying with recursive bayesian estimation and attenuation modeling," *IEEE Transactions on Automation Science and Engineering*, 2020.

[28] M. R. Morelande and A. Skvortsov, "Radiation field estimation using a gaussian mixture," in *2009 12th International Conference on Information Fusion*. IEEE, 2009, pp. 2247–2254.

[29] D. Kim, H. Woo, Y. Ji, Y. Tamura, A. Yamashita, and H. Asama, "3d radiation imaging using mobile robot equipped with radiation detector," in *IEEE/SICE SII*, 2017.

[30] A. A. R. Newaz, S. Jeong, H. Lee, H. Ryu, and N. Y. Chong, "Uav-based multiple source localization and contour mapping of radiation fields," *Robotics and Autonomous Systems*, vol. 85, pp. 12–25, 2016.

[31] F. Mascarich, C. Papachristos, T. Wilson, and K. Alexis, "Distributed radiation field estimation and informative path planning for nuclear environment characterization," in *IEEE ICRA*, 2019.

[32] F. Mascarich, P. De Petris, H. Nguyen, N. Khedekar, and K. Alexis, "Autonomous distributed 3d radiation field estimation for nuclear environment characterization," in *2021 IEEE International Conference on Robotics and Automation (ICRA)*. IEEE, 2021, pp. 2163–2169.

[33] J. Aleotti, G. Micconi, S. Caselli, G. Benassi, N. Zambelli, M. Bettelli, and A. Zappettini, "Detection of nuclear sources by uav teleoperation using a visuo-haptic augmented reality interface," *Sensors*, vol. 17, no. 10, p. 2234, 2017.

[34] J. MacFarlane, O. Payton, *et al.*, "Lightweight aerial vehicles for monitoring, assessment and mapping of radiation anomalies," *Journal of environmental radioactivity*, vol. 136, pp. 127–130, 2014.

[35] P. G. Martin, S. Kwong, N. Smith, Y. Yamashiki, *et al.*, "3d unmanned aerial vehicle radiation mapping for assessing contaminant distribution and mobility," *International Journal of Applied Earth Observation and Geoinformation*, vol. 52, pp. 12–19, 2016.

[36] J. Han, Y. Xu, L. Di, and Y. Chen, "Low-cost multi-uav technologies for contour mapping of nuclear radiation field," *Journal of Intelligent & Robotic Systems*, vol. 70, no. 1–4, pp. 401–410, 2013.

[37] K. Kochersberger, K. Kroeger, B. Krawiec, E. Brewer, and T. Weber, "Post-disaster remote sensing and sampling via an autonomous helicopter," *Journal of Field Robotics*, vol. 31, no. 4, pp. 510–521, 2014.

[38] K. Kochersberger, J. Peterson, P. Kumar, J. Bird, M. McLean, W. Czaja, W. Li, and N. Monson, "Unmanned aircraft applications in radiological surveys," in *2018 IEEE International Symposium on Technologies for Homeland Security (HST)*. IEEE, 2018, pp. 1–5.

[39] S. Schraml, M. Hubner, P. Taupe, M. Hofstätter, P. Amon, and D. Rothbacher, "Real-time gamma radioactive source localization by data fusion of 3d-lidar terrain scan and radiation data from semi-autonomous uav flights," *Sensors*, vol. 22, no. 23, p. 9198, 2022.

[40] F. Mascarich, M. Kulkarni, P. De Petris, T. Wilson, and K. Alexis, "Autonomous mapping and spectroscopic analysis of distributed radiation fields using aerial robots," *Autonomous Robots*, vol. 47, no. 2, pp. 139–160, 2023.

[41] M. Werner, T. Báča, P. Štibinger, D. Doubravová, J. Šolc, J. Rusnák, and M. Saska, "Autonomous localization of multiple ionizing radiation sources using miniature single-layer compton cameras onboard a group of micro aerial vehicles," in *2024 IEEE/RSJ International Conference on Intelligent Robots and Systems (IROS)*, 2024, pp. 5710–5717.

[42] J. Gu, H. Wang, G. Ding, Y. Xu, and Y. Jiao, "Uav-enabled mobile radiation source tracking with deep reinforcement learning," in *2020 International Conference on Wireless Communications and Signal Processing (WCSP)*. IEEE, 2020, pp. 672–678.

[43] A. H. Liu, J. J. Bunn, and K. M. Chandy, "Sensor networks for the detection and tracking of radiation and other threats in cities," in *Proceedings of the 10th ACM/IEEE International Conference on Information Processing in Sensor Networks*. IEEE, 2011, pp. 1–12.

[44] M. I. Ahmad, M. H. Ab. Rahim, R. Nordin, F. Mohamed, A. Abu-Samah, and N. F. Abdullah, "Ionizing radiation monitoring technology at the verge of internet of things," *Sensors*, vol. 21, no. 22, p. 7629, 2021.

[45] A. Victor, S. Viorica, S. Anatoliy, R. Oleksiy, and I. Maykiv, "Mobile sensors network for detection of ionizing radiation sources," in *2015 IEEE 8th International Conference on Intelligent Data Acquisition and Advanced Computing Systems: Technology and Applications (IDAACS)*, vol. 2. IEEE, 2015, pp. 913–917.

[46] D. Turecek, J. Jakubek, E. Trojanova, and L. Sefc, "Single layer compton camera based on timepix3 technology," *Journal of Instrumentation*, vol. 15, no. 01, p. C01014, 2020.

[47] A. Haefner, D. Gunter, R. Barnowski, and K. Vetter, "A filtered back-projection algorithm for 4π compton camera data," *IEEE Transactions on Nuclear Science*, vol. 62, no. 4, pp. 1911–1917, 2015.

[48] T. Baca, D. Hert, G. Loianno, M. Saska, and V. Kumar, "Model predictive trajectory tracking and collision avoidance for reliable outdoor deployment of unmanned aerial vehicles," in *2018 IEEE/RSJ International Conference on Intelligent Robots and Systems (IROS)*. IEEE, 2018, pp. 1–8.

[49] D. Hert, T. Baca, P. Petracek, V. Kratky, R. Penicka, V. Spurny, M. Petrlik, M. Vrba, D. Zaitlik, P. Stoudek, V. Walter, P. Stepan, J. Horyna, V. Pitzl, M. Sramek, A. Ahmad, G. Silano, D. Bonilla Licea, P. Stibinger, T. Nascimento, and M. Saska, "MRS Drone: A Modular Platform for Real-World Deployment of Aerial Multi-Robot Systems," *Journal of Intelligent & Robotic Systems*, vol. 108, pp. 1–34, July 2023.